- Technical Paper -

NUMERICAL SIMULATION OF THERMAL CRACKING IN LONG RC WALLS OF SEWAGE TREATMENT PLANT

Adnan AKMAL[*1], Akira HOSODA[*2], Ngoc T. PHAN[*3], and Kouji YOSHIHIRO[*4]

ABSTRACT

This study examines a sewage treatment plant that exhibited many thermal cracks in its walls, resulting in costly repairs. The peripheral wall has the L/H ratio of 17.3, which is quite large compared to the wall-type structures externally restrained in general. Despite the use of a large reinforcement ratio of 0.83% and good construction practices, crack widths up to 0.35mm were observed. The Crack Equivalent Strain module of JCMAC3 is adopted to simulate this behavior. The temperature and cracking analysis results are compared with the actual temperature record, crack width and crack pattern.

Keywords: Long RC walls, base-restrained RC wall, sewage treatment plant, thermal cracking, FEM thermal analysis, crack equivalent strain method

1. INTRODUCTION

Thermal cracking is inevitable in mass concrete members undergoing volumetric changes at an early age while subjected to external restraint caused by the adjoining rigid body. Thermal cracks occur despite adopting the latest recognized design and construction practices due to the complex and simultaneous effect of many critical factors concerning semi-controlled material properties and environmental conditions. This phenomenon is quite evident in wall-type structures where the newly placed wall lift is restrained to volume change by the previously cast wall lift or base slab.

Thermal cracking is controlled by limiting the maximum allowable crack width prescribed to achieve the structural performance requirements. It is done by using several countermeasures, such as utilizing crack-controlling reinforcement and expansive additive in the concrete mix, etc. However, the crack control criteria are quite stringent for liquid retaining structures like the sewage treatment plant where the crack occurrence is undesirable to avoid leakages. The JSCE-Standard Specifications for Concrete Structures (Design) [1] and the ACI committee 224 recommend the maximum crack width (MCW) limit of 0.10mm for water tightness [2]. However, for the subject sewage treatment plant, the allowable limit of MCW is set to 0.20mm by the local authorities to prevent leakage.

In wall-type structures, external restraint is one of the major factors for tensile stress in the restrained wall-lift. Tensile stress varies depending on the distribution of restraint level along the member before and after cracking. There are different prevailing guidelines for the control of thermal cracking that commonly define the restraint level in relation to the relative geometry and stiffness of restrained lift and restraining base lift. The JCI-Guidelines for Controlling of Cracking of Mass Concrete 2016 (JCI-2016) defines the degree of external restraint K_R as a function of the ratio of height-length (H/L) of the restrained lift and the Young's modulus ratio (E_C/E_R) of restrained and restraining lifts. At a constant height, tensile stress decreases with the decrease in length due to a lower degree of restraint [3]. ACI committee 207 also relates the degree of external restraint with the structural shape restraint factor K_R and foundation restraint factor K_f, which represent the length-height ratio (L/H) of restrained lift and stiffness of restraining base respectively [4]. Hosoda et al. indicated a positive correlation between the degree of restraint (defined as a function of L/H and casting time interval of two lifts) and the MCW of the bridge abutment wall based on the actual data from the Yamaguchi Prefecture System [5], [6].

In general, the crack-control reinforcement is designed based on the commonly observed cracking patterns, where thermal cracks occur near the base and propagate upwards in bottom-restrained walls due to potentially larger restraint at the base. However, this design approach is not fully effective in controlling thermal cracking in long walls with large L/H ratio due to the structural and performance constraints, which exhibit many thermal cracks also originating from the top. This aspect of thermal crack control in large structures has not been significantly investigated in past research.

First, this study aims to simulate thermal cracking behavior in a large real structure showing many cracks in its walls, extending from top to bottom despite having a large reinforcement ratio. Later, it could lead to a more effective crack control design for large structures. The case of a large rectangular sewage treatment plant located in Yamaguchi, Japan, is considered. Its

*1 PhD Student, Graduate School of Urban Innovation, Yokohama National University, JCI Student Member
*2 Prof., Graduate School of Urban Innovation, Yokohama National University, JCI Member
*3 Lecturer, Department of Civil Engineering, University of Technology and Education, The University of Danang
*4 Civil Engineering Department, Katsui Construction Co., Ltd.

peripheral wall has L/H ratio of 17.30 and 8.50 in longer and shorter directions respectively. Most of the cracks are through cracks which reportedly occurred from the top of the wall near the mid-span. A reinforcement ratio of 0.83% was used but no expensive additive was used in the walls. The Crack Equivalent Strain (CES) module of JCMAC3 for calculating the crack width of discrete cracks is used for FEM numerical analysis [7], [8]. The results of temperature and cracking analysis of three different FEM models are compared with the actual record of temperature, crack width and crack pattern.

2. STRUCTURAL DETAILS OF THE SEWAGE TREATMENT PLANT

2.1 Geometry and Construction Sequence

The sewage treatment plant has a basement of 44.35×21.4×4.9m. The 3D layout of the basement is shown in Fig. 1. The outer walls are 600mm thick, while the inner walls have varied thicknesses between 250-400mm.

The basement is 5.8m below the groundwater table level, making it a submerged water-containing structure in groundwater. After the temporary construction of the cofferdam all around the area, a 200mm thick gravel layer was laid, followed by a 100mm thick plain concrete as a levelling layer. The base slab of 1200mm thickness was cast in a single step without any construction joint. The RC walls of 4.9m were cast in two consecutive lifts of 2.6m and 2.3m height. However, no vertical joint was considered during the concrete pouring of both wall lifts. The first lift was cast after 73 days of placing the base slab. The total concrete volume is 340m^3 and 350m^3 of first and second wall lifts, respectively, including all outer and inner walls. The base slab and first wall lift were cast in mid-June and early September 2022, respectively. Cracking behavior in the first lift of the outer wall is considered here which exhibited more severe cracking than in the second lift.

Within this study, a part of the structure considered in the analysis is highlighted, as described in Fig. 2(a).

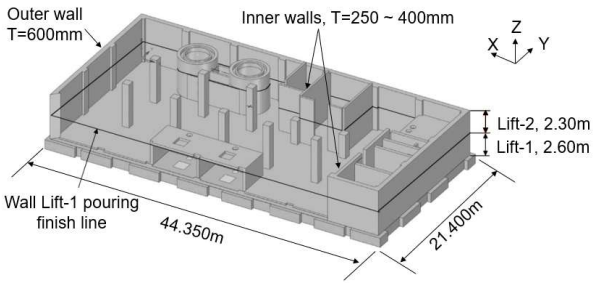

Fig. 1 3D Layout of the basement

2.2 Concrete Mix Design of Walls

The constituents of the concrete mix used in walls are given in Table 1, where W=water, C=cement (OPC), S=fine aggregate, G=coarse aggregate, and Ad=additive for achieving workability; the air content was set at 4.5%.

Table 1 Mix design for RC walls

W/C (%)	Air (%)	Unit weight (kg/m³)				
		W	C	S	G	Ad
54	4.5	173	321	971	895	2.89

2.3 Reinforcement Detail of Outer Walls

In the outer peripheral walls, a reinforcement ratio of 0.83% was employed to limit the MCW to 0.20mm based on the calculation method prescribed in the JCI-2016 guidelines. This ratio was increased from the original design [3]. Fig. 2(b) displays the arrangement detail of the outer wall reinforcement including added crack control rebars. Based on the generally observed

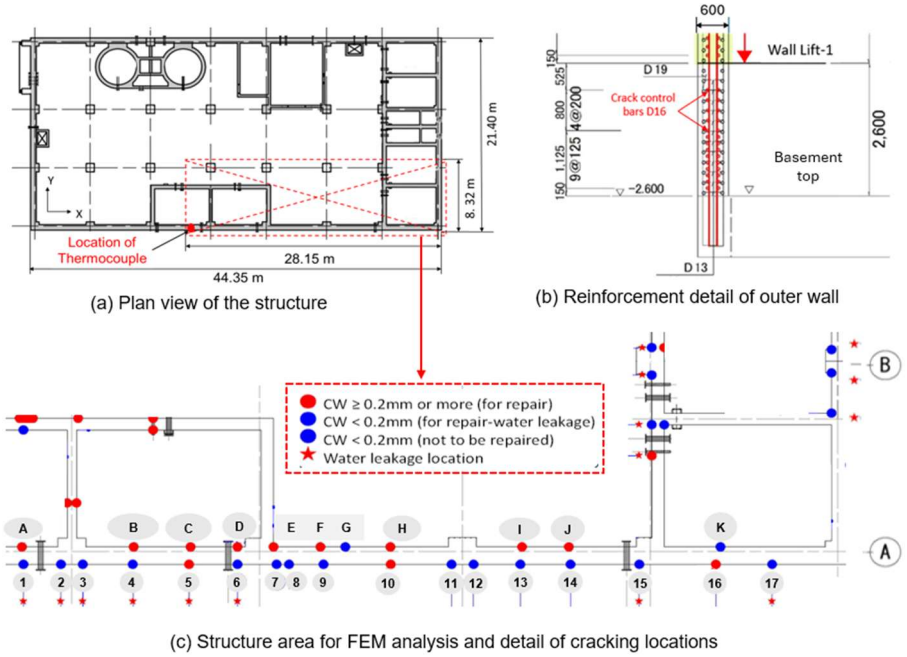

(a) Plan view of the structure

(b) Reinforcement detail of outer wall

(c) Structure area for FEM analysis and detail of cracking locations

Fig. 2 Reinforcement and cracking detail of the outer wall to be analyzed

thermal cracking patterns in most of the base-restrained walls where the cracks occur near the base and extend upwards, the design employed the smaller bar spacing of 125mm in the segment of 1275mm height near the base.

2.4 Crack Investigation Report

The initial crack survey was performed after two weeks, and the second crack survey was executed 1.5 months after the placement of the wall. The observed crack width in the first lift of the walls ranges from 0.05mm to 0.35mm. Subsequent reports found that most cracks extended vertically from top to bottom and only a few formed upward from the base area.

The location and category of crack according to width and water leakage are shown in Fig. 2(c). Cracking locations with a crack width (CW) of more than 0.20mm and subjected to repairs are shown as red circle dots. The cracking locations with CW less than 0.20mm are designated blue. Only those cracks with CW less than 0.20mm which showed water leakage after conducting the water leakage test were repaired. The leakage points are marked as red stars. The cracking locations of the first lift of the outer wall at grid-A on the outer and inner surfaces are designated with numbers (1-17) and letters (A-K) respectively, as shown in Fig. 2(c).

3. FEM ANALYSIS USING JCMAC3

3.1 Analysis modules of JCMAC3

The study utilizes FEM numerical simulation using commercial software of JCMAC3 [8]. It analyses the expansion and shrinkage behavior of the sewage treatment plant during its early age, focusing on thermal, stress, and crack width analysis. Drying shrinkage was not considered in this simulation. The analysis uses three-dimensional linear hexahedral elements and two-dimensional convective heat transfer elements. Furthermore, reinforcing bars were represented using one-dimensional truss components in both the longitudinal and transverse directions of the walls. The material properties obtained through the available construction data and certain parametric assumptions were utilized in the model.

The temperature distribution corresponding to each time is calculated in the temperature analysis. In the crack width analysis, cracks are represented by CES.

3.2 Crack Equivalent Strain Method

The smeared crack model is used for crack analysis, treating reinforced concrete as a continuum even after cracking. This approach eliminates the need to predict crack locations in advance and represents cracks as crack-equivalent strain.[7], [8].

3.3 FEM Model

The structure of the water treatment plant is quite large and unsymmetrical. The FEM model for the selected areas is shown in Fig. 3(a). The consideration of the area is to have at least half of the outer wall length that exhibited more severe cracking. Only the first lift of walls exhibits more cracking than the second lift, which is modeled as a 3D solid heat-generating component. The first wall lift is cast 73 days after the base slab, which is considered a fully hardened, non-heating restraining base in the model. Reinforcement bars are modeled as 1D truss elements, while the base slab is modeled without reinforcement, as shown in Fig. 3(c).

As shown in Fig. 3(b), the leveling concrete, gravel, and ground layers are non-heating components in the model. Fixed boundaries are applied in the X and Y directions at the cutting planes perpendicular to the longitudinal and transverse sides, while the ground bottom is fixed in all three directions (X, Y, and Z). 2D elements are used for surfaces exposed to ambient temperature changes over time. The mesh size for wall and base slab is set such that the region extending 200mm from the heat-transferring surface is divided into four elements with thicknesses of 5, 30, 65, and 100mm. The maximum element thickness is 300mm.

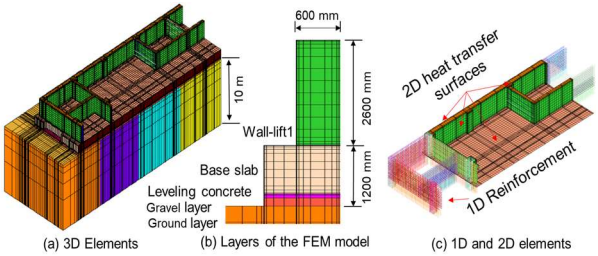

Fig. 3 3D layout and layers of the FEM model

3.4 Input Parameters for the FEM Analysis

In the temperature analysis, the initial temperature value of wall concrete and the ambient temperature history obtained from the construction record at the site is used. However, the initial temperature values for non-heating components such as the base slab, leveling concrete, and the ground are assumed as specified in Table 2. The 2D heat transfer exposed surfaces of the wall are given specific heat transfer coefficient (HTC) values according to the curing conditions adopted during the construction and considering the range specified in the JCI-2016 guidelines [3]. HTC values of 14 and 10 are used for wall-top and side surfaces respectively. HTC value 10 is changed to 14 from the time of demolding the formwork for the wall-side surface. HTC 14 is input for all the other heat transfer elements. The JCI-2016 model for adiabatic temperature rise, given as equation (1), was utilized in temperature analysis [3].

$$Q(t) = Q_\infty\left[1 - exp\{-r_{AT}(t - t_{0,Q})^{S_{AT}}\}\right] \quad (1)$$

where, Q_∞ represents the ultimate adiabatic temperature rise (°C) as a function of the unit cement content and the initial concrete placement temperature. $Q(t)$ denotes the rise of the adiabatic temperature in t days (°C). r_{AT} and s_{AT} denote the adiabatic temperature rise rate, influenced by the initial concrete placement temperature, while $t_{0,Q}$ marks the start of this rise.

The main thermal properties, such as the initial temperature, and coefficient of thermal expansion (CTE) are mentioned in Table 2. JCI-2016 time-dependent models for Ordinary Portland Cement (Normal Cement) are used to develop compressive strength, Young's modulus, and tensile strength of concrete.

The FEM stress analysis also incorporates creep

and autogenous shrinkage effects based on JCI-2016 guidelines for normal cement [3]. Cracking analysis is then conducted using the CES built-in module, as detailed in Section 3.

Table 2 Input thermal properties

FEM Layer	Initial Temperature (°C)	CTE (X10^{-6}/°C)
Ground	20	10
Gravel	20	10
Level concrete	20	10
Base slab	27.3, 29.3	10
RC Walls	27.3, 29.3	10

4. FEM ANALYSIS RESULTS AND DISCUSSION

4.1 Temperature Analysis

Three different FEM models (M1, M2, and M3) are analyzed based on varying input values of the initial concrete temperature (T_i) and adiabatic temperature rise Q_∞ for wall concrete. Additionally, the ambient temperature (T_a) is considered for the heat transfer surface elements. The differences in input conditions for these models are summarized in Table 3. In the analysis, the base slab initial temperature is set to T_i =29.3°C for M1 and T_i =27.3°C for M2 and M3.

Table 3 Difference in the input conditions

Model	Input parameters for wall		
	T_i (°C)	T_a data	Q_∞ (°C)
M1	29.3	Site + JMA	52.5 (JCI)
M2	27.3	Site + JMA	52.5 (JCI)
M3	27.3	JMA	50 (assumed)

The actual placing of wall concrete was done in many small continuous pours with different T_i values to reach the full lift height of 2.6m from early morning to evening. T_i values range from 27.3°C to 31°C with an average of 29.3°C as recorded. However, it is complicated to consider such variation of T_i in the FEM analysis. Therefore, the wall concrete is placed in a single pour with a uniform input value of T_i in the analysis. An average value of T_i =29.3°C is used as input in the model M1. T_i =27.3°C is considered in the models M2 and M3. A period of 28 days from the wall placement is considered in the analysis.

Thermocouples were installed at the location (shown in Fig. 2 (a)) to measure the temperature development in the wall at center (TCC) and near the surface (TCS), and the outside ambient temperature T_a. The ambient temperature was recorded for the initial 5 days from the wall concrete placement. T_a from the nearest Japan Meteorological Agency (JMA) station, along with the site-recorded T_a, is used for the entire analysis period. The JMA data shows an average T_a 5°C lower than the site record. For the initial days, the site-recorded T_a is used for M1 and M2, while JMA T_a data is used for the entire analysis period in M3. T_a considered for each model is shown in Fig. 4(a). The comparison of measured concrete temperature for wall TCC and TCS; and the analysis results of concrete temperature at the wall center (TAC) and near the surface (TAS) is shown in Fig. 4(b), (c), (d) for the models M1, M2 and M3 respectively.

The analysis results of M1 show the maximum temperature at wall center TAC= 60.4°C as compared to TCC= 53.4°C measured at the site. However, better agreement is observed for the concrete temperature near the surface. TAC=58.8°C in the M2 where a smaller value of T_i =29.3°C is used. The value of Q_∞ obtained from the experiment of the actual concrete mix used at the site is not available. Therefore, the value of adiabatic temperature rise Q_∞ =52.4°C from the JCI-2016 model (Eq. 1) is used for M1 and M2. The temperature analysis of M1 and M2 showed a higher maximum temperature rise than the measured value, leading to larger crack widths. Therefore, Q_∞ is calibrated to 50°C allowing temperature and crack width analysis results of M3 to be compared with the actual measurements. Furthermore, T_a from the JMA station for the total analysis period is considered in M3.

The analysis results of M3 show a good agreement of the maximum temperature rise in concrete for TAC and TCC. However, the analysis temperature decreased at a relatively faster rate than that of the actual measured temperature during the cooling phase of concrete. The observed temperature differences between the analysis and measured values could have resulted from the possible discrepancies in the assumed input parameters of the adiabatic temperature rise and HTC for which the experiment data is not available.

4.2 Crack Width Analysis

Fig. 5 compares the crack width analysis results of the models M1, M2, and M3. The CES (ε) as contours represent each discrete crack in the vertical direction

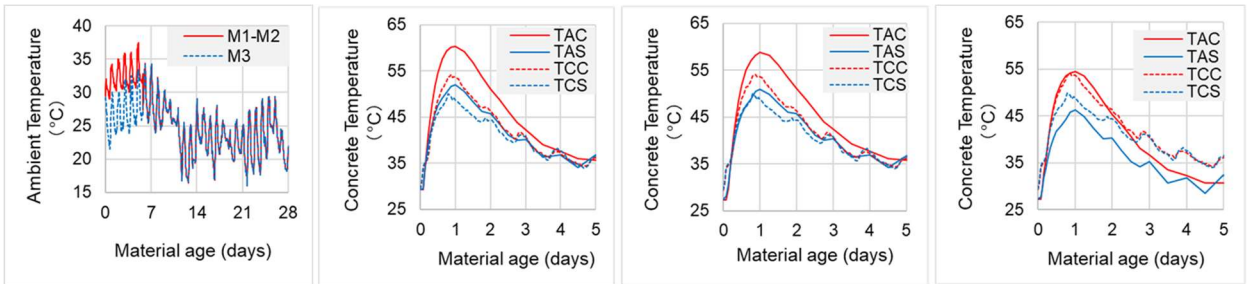

(a) Ambient Temperature (b) Concrete Temperature - M1 (c) Concrete Temperature – M2 (d) Concrete Temperature – M3

Fig. 4 Comparison of temperature analysis results of three different models

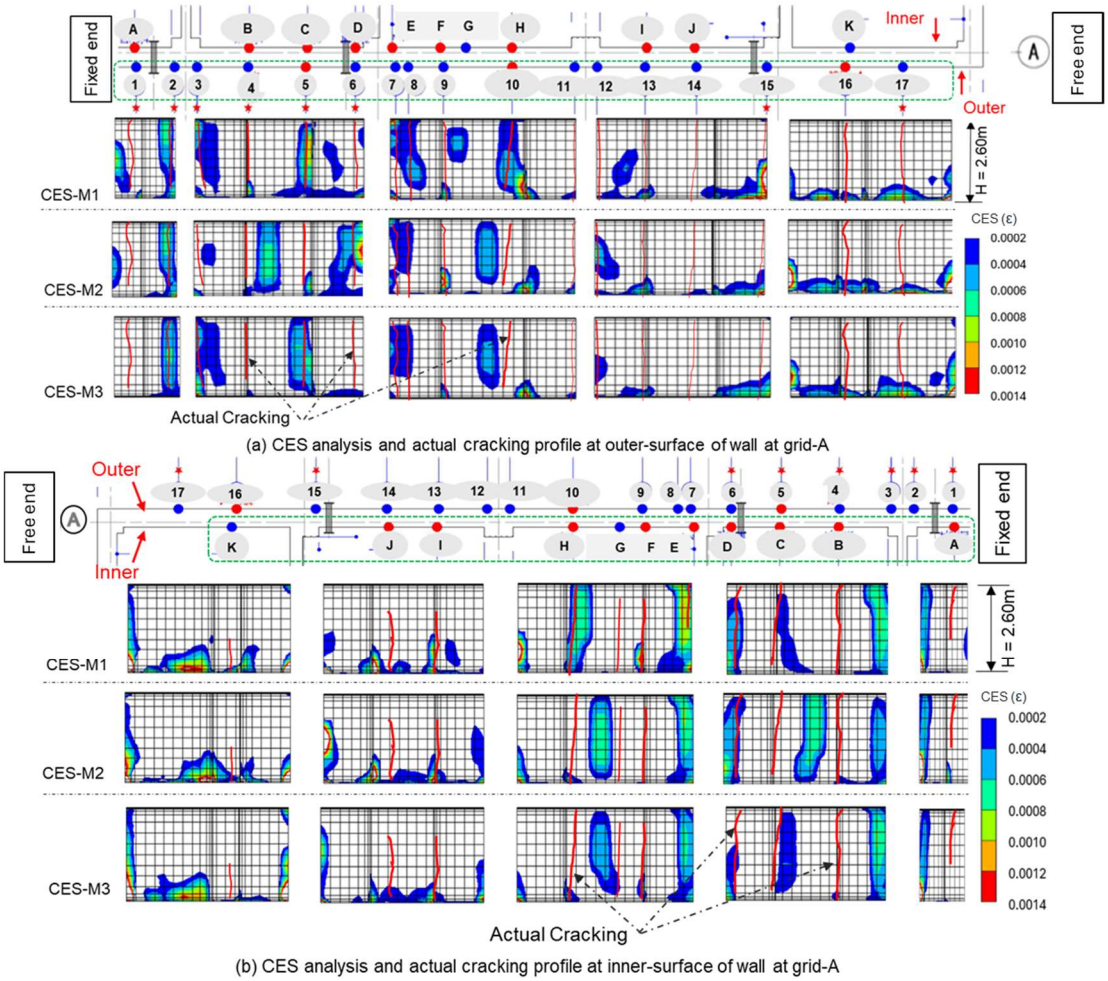

Fig. 5 Comparison of CES and the actual cracking pattern

along the height H=2.6m of the wall at grid A. Fig. 5 (a) and Fig. 5 (b) show the CES from each model at the outer and inner surface of the wall respectively. The red-marked lines show the cracking pattern recorded in the crack investigation report. From the actual cracking pattern (red lines) and the cracking location (red and blue marks), it can be noted that more cracks (A-K) with CW≥0.20mm occurred at the inner surface of the wall than at the outer surface. Most cracks (1-17) at the outer surface have CW<0.20mm.

Furthermore, it is also evident that about 50% of the actual cracks occurred near the fixed end of the FEM model (mid-span of total wall length at grid A) at both the inner and outer surfaces of the wall. Fig. 5 also shows that the CES in M2 and M3 develops from the top to the bottom of the wall, which closely resembles the actual cracking pattern observed at locations on both the outer and inner surfaces of the wall. However, 50% of the total actual cracks near the free end are generated from the base of the wall, with some cracks reaching full wall height, for example in the case of cracks observed at the outer surface. Fixed and free ends are referred to as the wall ends given fixed and free boundary conditions respectively in the FEM analysis as shown in Fig. 5.

The CES results obtained from the FEM analysis of M1, M2 and M3 also show quite similar patterns as that of actual cracking at most of the locations near the fixed end of the model on both surfaces. From the simulation results, relatively larger CES can also be

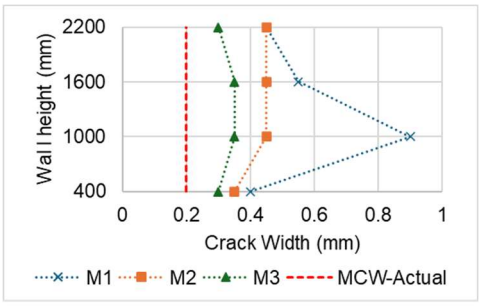

(a) MCW on outer surface of wall

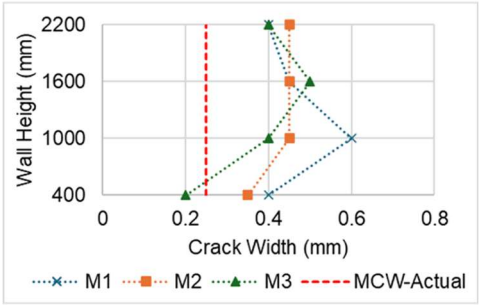

(b) MCW on inner surface of wall

Fig. 6 Comparison of MCW on the outer and inner surface

observed near the top of the wall at the sections closer to the fixed end. However, the total number of discrete crack locations from the analysis is somehow less than that of the actual cracks. CES values and potential crack locations decrease from M1 to M3, reducing maximum crack width along the height from 400mm to 2200mm (calculated by the CES method). Fig. 6(a) and (b) show this for outer and inner surfaces. The simulated MCW remains larger than the measured MCW in all models.

As the FEM model considers about half of the total wall length at grid-A, the above cracking behavior can also be explained considering the total wall length of 44.35m and the corresponding L/H=17.3. At a constant wall height, the smaller wall length fixed at the base will cause relatively less restrained stress at the top free end of the wall than near the bottom fixed end. Therefore, as the L/H ratio increases in the case of a long wall, the top free end also comes under the high restrained-stress zone. This results in the crack generation from the top free end at the first. However, as more secondary cracks occur near the mid-span of the long wall and tensile stress decreases around the crack vicinity, the effective L/H ratio gradually decreases in the other uncracked parts of the wall. This results in more distributed cracks with relatively smaller CW generated from the bottom near the side ends of the wall.

Kheder et al. explained this effect by developing idealized change of restraint diagrams for walls with varied L/H ratios (1-8) using two-dimensional finite element analysis and verified it with experimental data. The authors also mentioned that in walls with L/H ratio greater than 5, crack width increased from the bottom to the top of the wall. MCW occurred at 20–40% of wall height for L/H ratios below 5 [9], [10]. Shehzad et al. noted MCW location shifts with L/H ratios from 1–12 and reported an upper L/H limit of 4 for most externally restrained walls [11].

However, due to structural requirements, limiting the L/H ratio and adhering to standard crack-control reinforcement practices in large wall-type structures is not always feasible. Therefore, this study could contribute to the effective design of crack-control reinforcement and other countermeasures for mitigating thermal cracking in long RC walls.

5. CONCLUSIONS

A severe case of thermal cracking in the long RC walls of a sewage treatment plant is simulated. Temperature and crack width analyses are carried out through three different FEM models. The simulation results are compared with the actual recorded concrete temperature development and the observed cracking pattern in the wall. The following conclusions can be drawn from this study:

(1) The general practice of providing crack-control reinforcement in the base-restrained walls following the concept of larger restrained stress near the base is not feasible for walls with a large L/H ratio.
(2) The FEM models showed quite similar cracking patterns to the actual situation e.g. cracks generated from the top at most of the locations near the fixed end of the wall on both surfaces.
(3) Relatively large values of the maximum crack width are obtained by the FEM models as compared to measured values, likely due to a smaller number of distributed cracks in the model than in the actual wall.

The variation in thermal input parameters in M1, M2, and M3 had a significant effect on the crack equivalent strain and maximum crack width. Therefore, further refinement of the FEM model is necessary, with a more sophisticated selection of input parameters.

ACKNOWLEDGEMENT

The authors are very grateful to Mr. Yuto YOSHIDA and acknowledge his valuable contribution and guidance in structural modelling for the FEM analysis.

REFERENCES

[1] “Recommendations for Practice of Crack Control in Reinforced Concrete Building (Design), pp. 259, 2022 (in Japanese).
[2] ACI-Committee-224, “Control of Cracking in Concrete Structures,” American Concrete Institute, 2001.
[3] “JCI Guidelines for Control of Cracking of Mass Concrete”, Japan Concrete Institute, Tokyo, 2016.
[4] ACI-Committee-207, “Effect of Restraint, Volume change, and Reinforcement on Cracking of Mass Concrete,” American Concrete Institute, 1995.
[5] A. Hosoda, A. Akmal, M. Saleem and Y. Yoshida, “Improvement of Artificial Neural Network Model for Thermal Crack Width in RC Abutments using Actual Construction Data” JCI Annual Proceedings, pp. 970-975, vol 44, No. 1, 2022.
[6] A. Hosoda, A. Akmal, Y. Yoshida and M. Saleem, “Prediction of Maximum Crack Width by Machine Learning using Concrete Construction Data in Yamaguchi System” AI and Data Science Papers, pp. 898-905, vol. 3, No. J2, 2022.
[7] “JCMAC3 Crack Width Analysis (JCSCW)”, JCI, User Instruction Manual, pp. 10-28, ver. 4.1, 2017.
[8] Y. Ishikawa, H. Ohashi, T. Tanabe., (2009). “Proposal of a Crack Width Evaluation Method using a Smeared Crack Model.” JCI Annual Proceedings, pp. 1555-1560, vol. 31, No. 2, 2009 (in Japanese).
[9] G.F. Kheder, “A New Look at the Control of Volume Change Cracking of Base-Restrained Concrete Walls,” ACI Materials Journal, pp. 262-270, vol. 94, S24, 1997.
[10] G.F. Kheder, R. S. Al Rawi and J. K. Al Dhahi, “Study of the Behavior of Volume Change Cracking in Base-Restraint Concrete Walls,” ACI Materials Journal, pp. 150-157, vol. 91, M13, 1994.
[11] M. K. Shehzad et al., “Investigation of the Influence of External Edge Restraint on Reinforced Concrete Walls,” AToMech1, Materials Research Forum LLC, pp. 622–633, 2023.